JOURNAL OF THE KOREAN ASTRONOMICAL SOCIETY
36: S63 ~ S73, 2003

SOLAR MICROWAVE BURSTS AND ELECTRON KINETICS

JEONGWOO LEE[1], SU-CHAN BONG[2], AND HONG SIK YUN[2]
[1]Physics Department, New Jersey Institute of Technology, Newark, NJ 07102, USA
E-mail: leej@njit.edu
[2]Astronomy Program, SEES, Seoul National University, Seoul 151-742, Korea

ABSTRACT

Solar flares present a number of radiative characteristics indicative of kinetic processes of high energy particles. Proper understanding of the kinetic processes, however, relies on how well we can separate the acceleration from transport characteristics. In this paper, we discuss microwave and hard X-ray bursts as a powerful tool in investigating the acceleration and transport of high energy electrons. After a brief review of the studies devoted to the kinetic process of solar flare particles, we cast them into a simple formulation which allows us to handle the injection, trap, and precipitation of flare electrons self-consistently. The formulation is then taken as a basis for interpreting and analyzing a set of impulsive and gradual bursts occurred on 2001 April 6 observed with the Owens Valley Solar Array, and HXT/WBS onboard *Yohkoh* satellite. We quantify the acceleration, trap, and precipitation processes during each burst in terms of relevant time scales, and also determine ambient density and magnetic field. Our result suggests that it should be the acceleration property, in particular, electron pitch angle distribution, rather than the trap condition, that is mainly responsible for the distinctive properties of the impulsive and gradual flares.

Key words : Sun: flares — Sun: radio radiation — Sun: magnetic fields — radiation mechanisms: nonthermal

I. INTRODUCTION

During solar flares, charged particles are accelerated to high energies, and their interaction with ambient plasma and magnetic field produces electromagnetic emissions under various radiation mechanisms. Among these, hard X-rays (HXRs) and microwave radiations (MWRs) are largely contributed by electrons accelerated to energy range of several tens of keV to MeV, via the mechanisms of Bremsstrahlung and synchrotron radiation, respectively (Melrose 1980). Since this is the most abundant species among the solar flare accelerated particles, the HXR and MWR have been regarded as the most powerful diagnostics for exploring physical processes that control the evolution of the electrons in phase space (Miller et al. 1997). In general, the modulation is not only due to the accelerator itself but also to other physical processes encountered after acceleration (Petrosian 1990; Aschwanden 2003). It therefore appears as an essential step to separate the radiation characteristics determined by the electron acceleration mechanisms from those by transport effects.

The very first theoretical formulation of the transport problem was implemented by Takakura & Kai (1966) in an application to MWR spectral evolution. This type of model can be regarded as a perfect trap model, since it considers the evolution of the electron energy distribution within a confined volume. However, electrons can escape out of the magnetic trap due to finite loss cones in real solar magnetic loops. Melrose & Brown (1976) formulated a system of trap and precipitation in order to treat the thin and thick target Bremsstrahlung altogether, which has been popularly used in interpretation of time and spectral variations of HXRs and MWRs (Aschwanden et al. 1997, and references therein). Later development of the transport problem have, however, been made mainly to explain the observed time delays between the HXR peaks at different energies. Bai & Ramaty (1979) and Bai (1982) interpreted the progressive delay of HXR peaks with higher energy as due to the effect of Coulomb collisions on the trapped electrons (see also Vilmer, Kane, & Trottet 1982). While the precipitation in Melrose & Brown's (1976) model refers only to the leakage from the trapped electron population ('secondary precipitation' hereafter), in many events there appears to be a need for electrons that directly precipitate into the chromosphere with little or no trapping. Aschwanden and coauthors (Aschwanden 1998; Aschwanden, Schwartz, & Dennis 1998; Aschwanden et al. 1999) present a time-of-flight model in which the directly-precipitating electrons are distinguished from the secondary precipitating electrons by looking at whether the HXR time delays occur toward lower energy as a result of the time-of-flight or toward higher energy due to Coulomb collisions in the trap.

MWR studies on the transport problem have followed in a way to complement the HXR observations. The most commonly discussed in this line would be the relative time profiles of HXR and MWR. In general, lightcurves of MWR and HXR share an overall

Corresponding Author: J. Lee

similarity, but the peak of MWR is a bit delayed and decay is a bit extended (e.g., Crannell et al. 1978; Cornell et al. 1984). These relative differences between MWR and HXR led to the idea that the observed radiation involves either an energy-dependence of the two radiations or a trap-related electron dynamics. A more systematic study was carried out by Lu & Petrosian (1988) who found two types of delays between 17 GHz and HXR: a short and relatively longer delays, which they interpreted as due to transport and acceleration effect, respectively. Melnikov (1990, 1994) investigated the relative fluxes and relative time delays between MWR and HXR as evidence for the energy-dependent trapping under Coulomb collisions (see also Melnikov & Magun 1998, Silva et al. 2000). Bruggmann et al. (1994) analyzed time delay between MWR peaks at different frequencies and the decaying lightcurves as due to Coulomb collisions and Betatron deceleration.

In more recent studies of electron transport, not only the energy-dependent evolution but also the electron pitch angles and influence of magnetic mirroring have been addressed. Lee & Gary (2000) and Lee, Gary, & Shibasaki (2000) have analyzed a burst of which spectral evolution is due to collisional energy loss plus pitch angle diffusion. Kundu et al. (2001a) studied time profiles of simple impulsive MWR bursts in comparison with HXR lightcurves, and explained the relative difference in terms of trap-and-precipitating picture by Melrose & Brown type, including the directly precipitating electrons. Lee et al. (2002) studied an impulsive event with rather a long tail, for which the direct precipitation hypothesis is found appropriate not only for the time profile similar to HXR but in explaining time-dependent injection spectrum on the optically thick MWR.

The electron transport problem has also been discussed with imaging observations. Many of the VLA observations of solar flares shows that MWR source often starts at the location of the loop top while the footpoint is more favorable for MWR emission due to strong fields there, which is sometimes regarded as a signature for acceleration (see, review by Marsh & Hurford 1982). Petrosian (1982), however, presented a more general consideration of a MWR loop-top source, involving the radiation transfer effect and particle kinetics in the presence of Coulomb scattering and magnetic mirroring. Holman, Kundu, & Papadopoulos (1982) proposed an idea that the loop-top source (Marsh & Hurford 1982) occurred because of an instantaneous trap of the high pitch-angle electrons and subsequent pitch angle diffusion. Kundu et al. (1995) observed an asymmetric MWR sources and interpreted it as due to asymmetric precipitation of nonthermal electrons, in harmony with Sakao's (1994) result for HXR. The asymmetric MWR source presented by Lee, Gary & Shibasaki (2000) and Lee & Gary (2000) also indicated the weak pitch-angle diffusion during the flare. Melnikov et al. (2002) studied MWR loop-top sources at 17 or 34 GHz, which are found to represent an actual concentration of electrons, which is consistent with the conclusions made by Holman et al. (1982) and Lee & Gary (2000). Another type of imaging approach has been made by Hanaoka (1996, 1997), Nishio et al. (1997), and Kundu et al. (2001b) in which Nobeyama 17 GHz imaging data together with HXR images from the *Yohkoh* satellite are used to evidence magnetic reconnection of multiple loops by looking at the double response at the footpoints connected to the injection point. More recently, Lee et al. (2003) reported evidence of spontaneous reconnection based on the spatial coincidence of the MWR sources with the magnetic separatrix.

In addition to time, spectral, and spatial morphologies, several authors investigated correlations of the MWR flux with proton flux (Bai 1986) and HXR flux (Kai, Kosugi, & Nitta 1985; Kosugi, Dennis, & Kai 1988; Melnikov 1990, 1994). These authors intend to explain the nature of the impulsive and gradual flares (Bai & Sturrock 1989) in terms of differing conditions in the trap. As a related study, Kosugi, Dennis, & Kai (1988) investigated correlations of HXR photon energies with 17 GHz MWR flux in an attempt to determine the effective energy of the MWR emitting electrons. Kai (1986) proposed an idea of the direct precipitating electrons to resolve the problem of inconsistent numbers of electrons deduced from HXR and from MWR, respectively. Klein, Trottet, & Magun (1986) demonstrated that use of a common injection function for both HXR and HXR can help resolving the number problem too. A physics emerging from these studies is that Coulomb collisions has a profound effect on dynamical evolution of electrons in energy space.

In this paper we present a new paradigm in which the electron pitch angle and ambient magnetic field are the important factors in determining the kinematics of electrons in the trap-and-precipitation system. We will then apply the paradigm to a set of impulsive and gradual bursts for a physical interpretation of the nature of these two classes of solar flares.

II. THE PROPOSED APPROACH

The problem that we intend to address, the acceleration and transport of particles, has a fundamental difficulty in that it is ambiguous to differentiate between the acceleration and transport effect in a given observation. As we will demonstrate here, the ambiguity can be reduced to some extent if we incorporate the finite magnetic field and the electron pitch angle into the problem. These two important parameters have largely been ignored in the conventional paradigm in which the emphasis is given to the electron energy and ambient density. In this section we build a simple formulation in order to illustrate the recent and past picture of trap and precipitation in a unified fashion.

The study of solar high energy particles considers a physical system in which electrons are injected into a trap by the quantity Q and leave the trap at a rate ν,

in which case the Fokker-Planck equation will be in the form:

$$\frac{\partial N}{\partial t} = [...] - \nu N + Q \quad (1)$$

where [...] should include all the variations in momentum and space. The solution to this equation takes a form of $N = K \otimes Q$, where the kernel function K accommodates all the terms in the right hand side except the injection. Our problem is therefore how to deconvolve Q from the resulting electron distribution function N, if the latter is obtained from observed radiation. In general all these quantities N, Q, and K involve time, energy and pitch angle as arguments, and not only the solution but even the formulation is hardly expressed in a convenient closed form. Here we consider a simple case where all the terms in [...] can be ignored, which corresponds to a collisionless trap where there is no loss of particles other than that due to escape (νN) and its pitch angle-dependence is implicitly handled. In this case the kernel function is simply an exponential function, and solution for trapped electrons is in the form $N = \int_0^t e^{-\nu(t-t')} Q(E,t')dt'$ where the transport effect is solely described by the property of the escape rate ν (Aschwanden 1998, Kundu et al. 2001a, Lee et al. 2002).

The trap-and-precipitation model owes to Melrose & Brown (1976) which introduces a precipitating region (thick target) attached to the trap region (thin target) from below. In this case, the escape rate ν therefore is the precipitational rate, which becomes another injection rate into the thick target region. With the present parameters, this idea can be expressed by:

$$\begin{aligned} N &= \int_0^t e^{-\nu(t-t')} Q(E,t')dt' \\ n &= \nu N(E,t) \end{aligned} \quad (2)$$

where N is the number of the trapped electrons and n is number of electrons, per unit time, injected into the thick target region. As a major advantage, the thick and thin targets are, in this idea, related to each other via the physics of pitch angle scattering, and ν is the central quantity which entirely controls the lives of the trapped electrons (N) and precipitating electrons (n). There are, however, a few limitations with this model. Since $n \propto N$, the trapped electrons ($\sim n$) is perfectly correlated with thick target electrons ($\sim N$) in time provided the comparison is made at same energy, whereas HXR are observed more impulsive than MWR.

An important step was forwarded by Aschwanden (1998) in which the population associated with direct precipitation is included into the above trap-and-precipitation system. To illustrate this idea, we split, the injected particles Q into two parts, according to whether the initial pitch angles are greater or smaller than the loss-cone angle, i.e., $Q(\phi \geq \phi_L)$ and $Q(\phi < \phi_L)$ (cf. MacKinnon 1991). Here the loss-cone angle, ϕ_L, is determined by the magnetic mirror ratio of the flaring loop, $\phi_L = \sin^{-1}(B_1/B_2)$, with B_1 and B_2 representing the magnetic field strength at the loop top and a footpoint, respectively. Since the particles with $\phi < \phi_L$ can directly precipitate without being trapped, (2) will be modified to the following form:

$$\begin{aligned} N &= \int_0^t e^{-\nu(t-t')} Q(E, \phi \geq \phi_L, t')dt' \\ n &= Q(E, \phi < \phi_L, t) + \nu N \\ &\equiv n_Q + n_N. \end{aligned} \quad (3)$$

It will be worthwhile to note that (3) will reduce to (2) in the limit of $\phi_L \to 0$, i.e. all particles are once trapped and then are able to precipitate. This is incorrect because there will be particles directly precipitate without being trapped. We can thus say the formulation (2) is valid to the extent that ϕ_L is ignored. The third formulation (3) is also imperfect, of course, since it does not explicitly describe any energy and pitch angle change during the trap, but it shows, on a minimum basis, how magnetic field and pitch angle distribution comes into the context of trap and precipitation. Under this model, we can deal with the following issues. A portion of injection function $Q(\phi < \phi_L)$ can be subject directly to observations, rather than treated as ever unknown. Also the magnetic field comes into the context, at least, in the form of mirror ratio. More importantly, the trapped and the precipitating populations may show differing time behaviors if the radiation from the new term $Q(\phi < \phi_L)$ dominates that from νN. As a result, we can have impulsive HXR and more extended MWR, even though they are emitted by same energy electrons. In the next we will utilize these ideas in analyzing a set of impulsive and gradual bursts.

III. DATA AND ANALYSIS

We study the X5.6 flare occurred on 2001 April 6 at 19:14–19:40 UT in the active region AR 9415. During this flare a set of impulsive and gradual bursts occurred, which were well observed at MWR and HXR wavelengths. MWR data were obtained with the upgraded Owens Valley Solar Array (OVSA), of which configuration included two solar-dedicated 27 m parabolic dishes and four 2 m dishes (Gary & Hurford 1999). The HXR data are from Hard X-Ray Telescope (HXT) and Wide Band Spectrometer (WBS) onboard *Yohkoh*, which provide imaging and spectral data, respectively (Kosugi et al. 1991; Yoshimori et al. 1991). In addition, EUV and UV images of the active region were obtained with TRACE before and after the flare, which provides high spatial resolution (2″) images of the solar chromosphere, transition region and corona. Magnetic field and continuum in the photosphere are obtained from the Michelson Doppler Imager (MDI) (Scherrer et al. 1995) onboard the *SoHO* which records high resolution (4″) magnetograms, dopplergrams, and line-depth images of the photosphere in the Ni I 6768 Å absorption line.

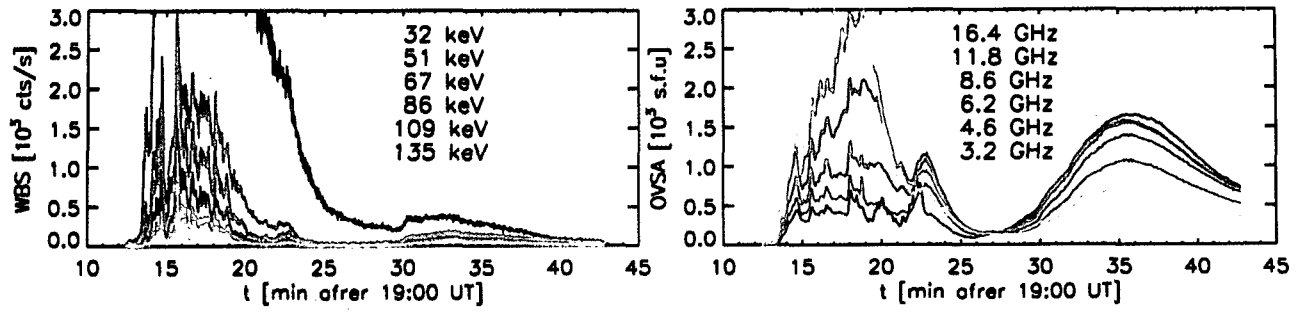

Fig. 1.— The HXR and MWR emissions during the large 2001 April 6 flare. The left panel shows the HXR lightcurves at selected HXR photon energies obtained from Yohkoh/WBS. The right panel shows MWR fluxes at selective frequencies from the OVSA.

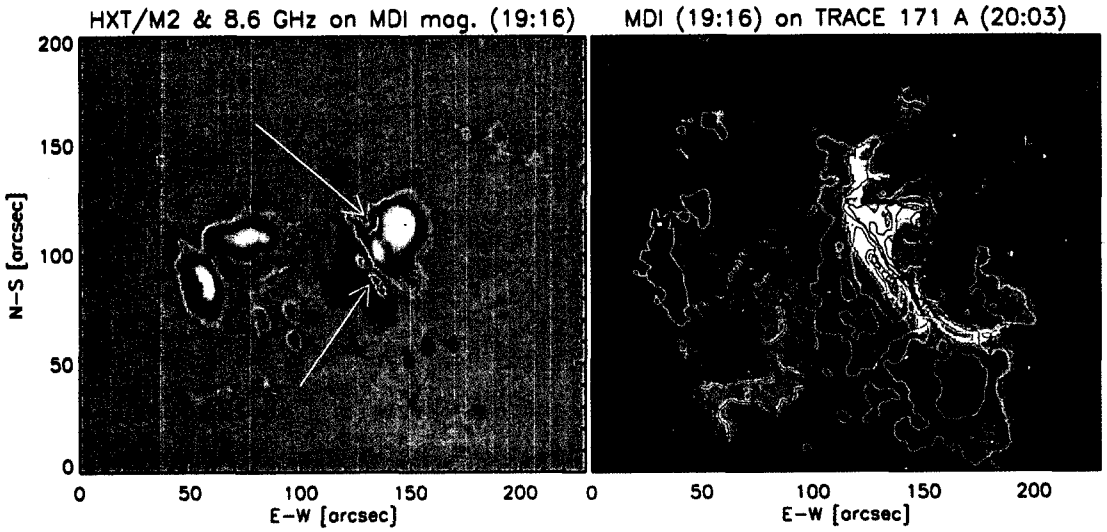

Fig. 2.— Magnetic field and EUV emission of the flare region, NOAA 9415. The left panel shows an MDI magnetogram during the impulsive phase in which the white and black features represent longitudinal magnetic field in positive and negative polarities, respectively. The arrows indicate the positions of the magnetic anomaly as discussed in the text. The right panel shows a TRACE EUV image at 171Å taken after the flare. Overlaid contours are longitudinal magnetic fields from the MDI magnetogram. The bright EUV emission occurs along the magnetic neutral line in the bipolar part of the active region.

(a) Lightcurves and Morphology

In Figure 1 we plot the lightcurves of HXR (left panel) and MWR (right panel) at selected photon energies and frequencies. The time resolution is 1 s for the HXR data and 4 s for the MWR data. The energies shown in the left panel are the medians of each energy channel of the WBS/Yohkoh. The time profiles show that the event consists of two bursts. The first burst (19:14-19:30 UT) consists of a number of short-period spikes and is regarded as an impulsive burst. The second burst (19:30 -19:40 UT) shows a smooth rise and fall, typical of a gradual burst. During the impulsive burst, a number of sharp HXR peaks appear simultaneous with the corresponding MWR peaks. On the other hand, during the gradual phase, a gradual time delay is seen from low to high energies in HXR and from HXR to MWR. It is also apparent that during the impulsive phase HXR flux is relatively stronger, while during the gradual burst MWR flux is much stronger (called microwave excess). All these properties are known typical for the impulsive and gradual bursts (e.g., Kosugi et al. 1988).

Figure 2 shows morphological properties of the active region. At the flare time, the active region was located at S21° E31°. The left panel shows a longitudinal magnetogram taken during the impulsive phase. As indicated by the arrows, a pair of unusually strong magnetic anomaly (Zirin & Tanaka 1981), a transient appearance of one magnetic polarity in the middle of the other polarity fields on a magnetogram, is observed during the impulsive phase. Interestingly, HXR sources appear in double sources at the same locations of these

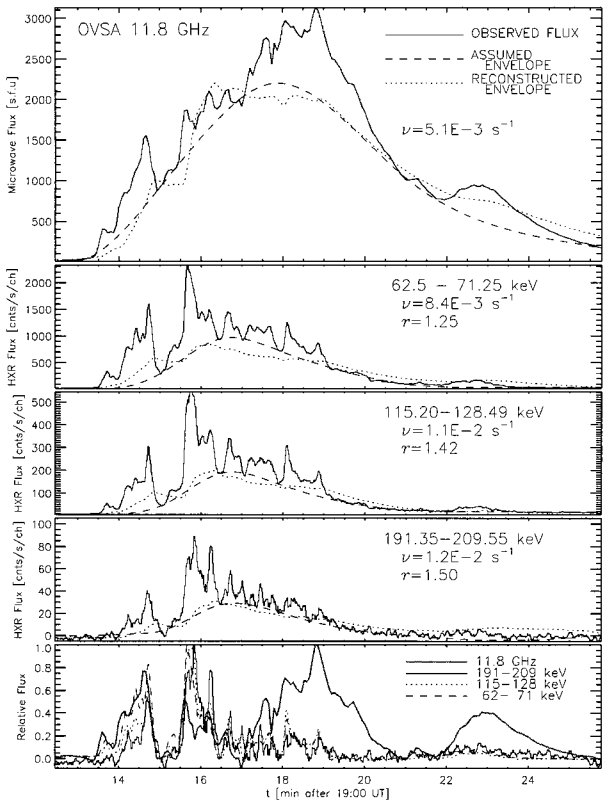

Fig. 3.— Analysis of the impulsive burst. The upper four panels show the lightcurves at 11.8 GHz from the OVSA and HXR at three energy channels from Yohkoh/WBS. In these panels, the solid lines are observed fluxes; the dashed lines are the envelopes underlying the impulsive peaks; the dotted lines are reproduced from the convolution of the fluctuation above the envelope with a kernel function. The parameters ν and r used for this fit are denoted in each panel. The bottom-most panel shows relative time profiles of the short-period fluctuations above the envelopes only.

two magnetic anomalies, and the MWR source is found in the middle of the magnetic anomalies. We did not overlay both HXR and MWR sources in the map because only the locations of these radiations relative to the magnetic transient are the most important in the present context. The right panel shows a TRACE image at 171 Å which includes the intense Fe IX and Fe X emission lines sensitive to plasma at temperature $\sim 1 \times 10^6$ K. We overlaid the longitudinal magnetic fields as contours in order to show the location of the EUV emission relative to the magnetic fields. The flare resulted a bright EUV feature aligned along the magnetic neutral line in the bipolar part of the active region, suggesting that magnetic fields in some arcade type structure are involved connecting the bipolar regions.

The magnetic transient phenomenon is considered as due to changes in line profiles caused by flare emissions (Zirin & Tanaka 1981). Recent study, which specifically addresses the spectral line used in the MDI magnetogram, has also indicated such possibility (Ding et al. 2002). Although the detailed process leading to the magnetic transient may still be in debate, it is important for our purpose that the HXR sources appear in the same locations of the magnetic transient. From this result, we can assure that the HXR should be associated with the precipitating electrons (n) rather than the trapped electrons (N) even for the gradual burst. This is an important clue to the hypothesis of the trap and precipitation system, because with the observed time behavior alone, we have no way to differentiate the trapped (N) and the secondary precipitating electrons (νN).

(b) Injection and Precipitation

Figure 3 shows the lightcurves of MWR and HXR during the impulsive burst at selected energy channels. The solid lines are observed fluxes, and the dashed and dotted lines in the top four panels are the envelope of the radiations. The bottom-most panel shows only the fluctuations. We shall shortly define the envelopes and fluctuations in the below.

The overall lightcurves of MWR and HXR shown in Figure 3 do not yield such an impression that they should be emitted by the same population of electrons. This is mainly because the MWR flux keeps increasing while HXR diminished after 15:16 UT. However, individual MWR peaks themselves are likely to be correlated with each other (see the bottom panel). The presence of both correlated and uncorrelated components is rather expected within the present formulation because the precipitation n consists of the fast variation associated with the direct precipitation, n_Q, and the slow variation associated with the secondary precipitation n_N (see Eq. [3]). Therefore the distinction between these two terms will be merely whether the flux lies above or below the envelope. In Figure 3, we thus set the envelope (shown as dashed lines) and regard the short period pulses above this envelope as the directly precipitating component (n_Q) and the underlying envelope as the secondary precipitating component (n_N).

The envelope shown in Figure 3 may look arbitrary. But we can require the assumed envelope to be self-consistent with the rest components in our model, because n_Q and n_N are under the following relationship:

$$\begin{aligned} n_N &= \nu \int_0^t Q(\phi > \phi_L, E, t) e^{-\nu(t-t')} dt' \\ &= r\nu \int_0^t Q(E, \phi \le \phi_L, E, t) e^{-\nu(t-t')} dt' \\ &= r\nu \, n_Q \otimes K. \end{aligned} \quad (4)$$

Here we introduced a parameter, r, the ratio of the electrons injected with pitch angles inside and outside of the loss cone, $r \equiv Q(E, \phi > \phi_L)/Q(E, \phi \le \phi_L)$. To guarantee this self-consistency, we adjust the level of the background and the value of ν until the reconstructed n_N (dotted lines) comes close to the original assumed envelope (dashed lines). A rough agreement between

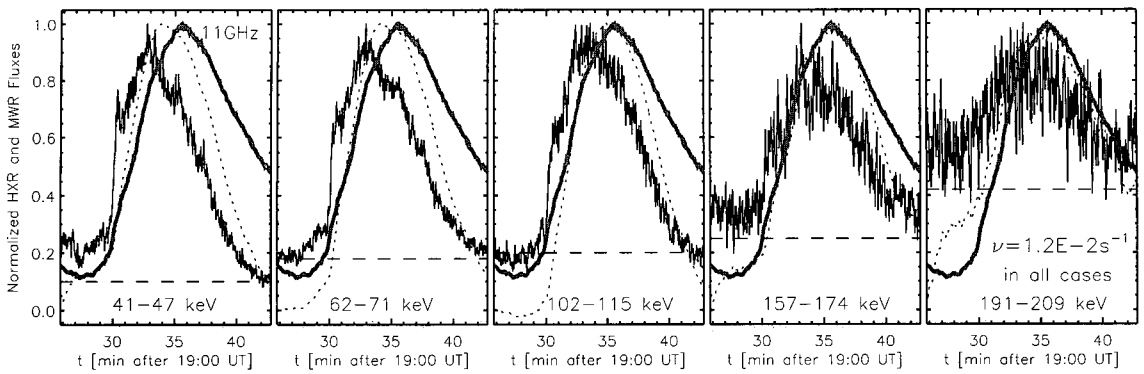

Fig. 4.— Relative lightcurves of HXR (solid lines) and MWR (grey-colored line) during the gradual burst, exhibiting an energy-dependent variation. At a closer look-at, we find that the HXR rises very rapidly at ~19:30 UT indicative of the onset of the acceleration whereas the slow decrease after ~19:36 UT suggests a decay associated with the convolution. The constant dashed line in each panel is the background taken for subtraction. The dotted line is a convolution of the net HXR flux with a kernel function, $\exp[-1.2 \times 10^{-2}\ t]$. At a low photon energy, this convoluted lightcurve falls before the MWR lightcurves, and at a higher energy (say > 180 keV) it approaches close to the MWR lightcurve.

the model fit and the observed HXR envelope is found at $\nu \approx 1.2 \times 10^{-2}$ s^{-1}. The derived values of ν and r show little variation across the HXR energy channels, and we do not believe that ν is an energy-dependent quantity. On the other hand, the MWR envelope is more extended and the fit is made at $\nu \approx 5.1 \times 10^{-3}$ s^{-1} which means a longer lifetime of MWR-emitting electrons compared with that of HXR electrons.

As to why so different ν results for MWR and HXR, we can consider two possibilities on a general ground. First, it could represent energy dependent variation of ν, assuming that MWR is emitted by higher energy electrons than HXR. Second, it could be that electrons emitting MWR and HXR reside in two different regions, respectively. The first hypothesis is considered unlikely in the present case, because no noticeable variation of ν across the HXR energy channels is seen. The second hypothesis is compelling because the MWR could be emitted by not only the precipitating electrons but also electrons trapped in the corona. Looking at the map in Figure 2, probably the MWR-emitting electrons are spread out all over the arcade loops, whereas the HXR-emitting electrons are concentrated to the two footpoints connected to the magnetic transient. Such separation can lead to a very different trap condition which is solely represented by the parameter ν in the present formulation.

(c) Energy-Dependent Trapping

We proceed to the second burst which shows a gradual time variation. Figure 4 shows the HXR lightcurves during the gradual burst at selected HXR energy channels together with an MWR at 11.8 GHz. We note that the burst extends about 8 min period without intermittent pulses. Here we will ignore the fine-scale fluctuations with ~2 s period, because they are also found even during the non-flaring times. The extended burst period could be entirely due to the emission property. Alternatively it can result as being moderated by a trapping process. In this regard, we note that the HXR flux starts to rise very abruptly at ~19:30 UT with an exponential time-scale ~30 s, which is much shorter than the whole period ~8 min. It is therefore likely that the whole burst actually consists of many short-period (≤1 min) peaks and they as a whole look like a single peak after being convolved with a kernel function.

We now turn our attention to the energy dependent trapping (Aschwanden & Alexander 2001). As a means to verify how the energy-dependence of the trapping plays a role, we investigate the convolution of the HXR with a kernel function in comparison with the observed MWR. Before convolution a constant background for the HXR flux (the dashed line in each panel) is taken out at each channel and this net HXR flux is convolved with an energy-independent kernel function given by $K(E,t) = \exp[-1.2 \times 10^{-2} t]$. The convolved quantity, $F_X \otimes K$, is plotted as a thick gray line in Figure 4. To compare with the MWR, these convoluted lightcurves fall before the MWR lightcurve at low photon energies and come closer to the MWR lightcurve at higher energies. This means that the HXR and MWR emitting electrons are again related to each other via a convolution, and that the dynamics is governed by an energy-dependent transport effect.

The precipitation rate, ν, in this case cannot be determined using the same method (Equation [4]), because during this gradual burst no discrete peak is identified as clearly as in the impulsive burst. Instead we assume, based on the observed time profiles, that the abrupt rise at ~19:30 UT signals the onset of acceleration, and the flux increase rate at this time, $\nu_a \sim 1/(30$ s), should be close to the acceleration rate. Such a short acceleration time scale compared with the precipitation time scale (ν^{-1} ~300 s) means that the smoothly falling

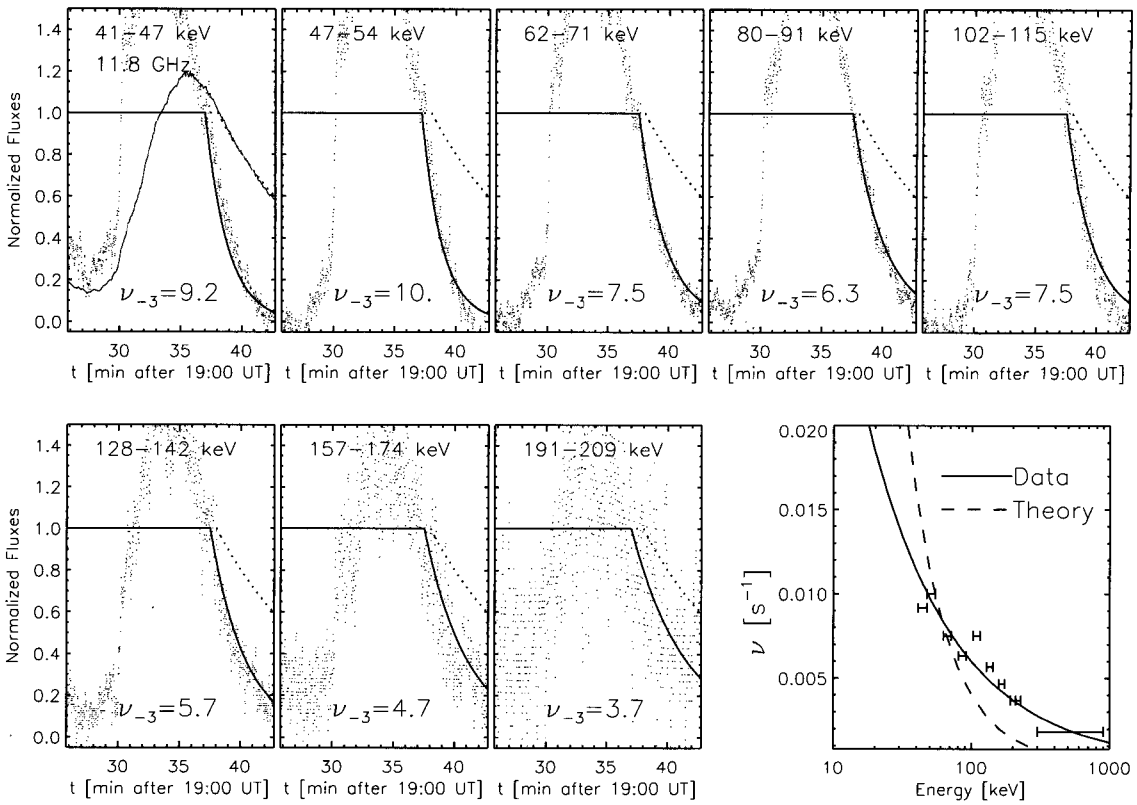

Fig. 5.— Analysis of the gradual burst. The smooth tail after ~ 19:37 UT is assumed to represent the kernel function $\exp[-\nu t]$ and is used to determine the parameter ν. The observed HXR and MWR fluxes are shown as dots, and the best-fit parameter in units of 10^{-3} s^{-1}, ν_{-3}, is given in each energy panel. The dotted line is a fit to the MWR 11.8 GHz, which is assumed to emitted by the electrons in 300–900 keV. The bottom-right panel shows the derived ν as a function of the photon energy. In this panel, the solid curve is a fit to the derived results, and the dashed line is a fit to the Coulomb deflection time-scale.

tail after ~19:37 UT is essentially shaped by the kernel function $\exp[-\nu t]$. More precisely, the tail profile would be represented by the following form:

$$N(t \geq t_0) \approx \frac{Q(t_0)}{\nu}\left[e^{-\nu(t-t_0)} - e^{-\nu_a(t-t_0)}\right] \quad (5)$$

where we set $t_0 \approx$ 19:37 UT as the ending time of acceleration. The acceleration history before this time, $Q(t < t_0)$, is relatively unimportant under this assumption. The result of fitting (5) to the observed lightcurves (dots) is shown as solid lines in Figure 5. The dashed line is a fit to the tail of the MWR lightcurve. In the bottom right panel, we plot the derived values of ν as a function of energy. The solid guide line in this panel shows that our results are well fitted to the form of $\nu \sim \epsilon^{-0.8}$, which therefore does not exactly agree to Coulomb deflection time. For comparison, however, we also made a fit of the result to the Coulomb deflection time scale, which is shown as dashed line in the same panel. This fit is in the form of $\nu \approx 6 \times 10^{-3}$ s^{-1} $(\epsilon/100$ keV$)^{-1.5}$. Note that for this gradual burst, the values of ν range from (0.41–1.1)$\times 10^{-2}$ s^{-1} in the energies 40-200 keV, which is smaller than the result for the impulsive burst by only a few factor.

(d) Trap Density and Magnetic Field

When the precipitation rate ν is found to vary with energy in accordance with the Coulomb deflection time scale, the ambient density in the trap can be determined by:

$$\nu_c \approx \frac{1.1}{\text{s}}\left(\frac{E}{100\text{ keV}}\right)^{-1.5}\left(\frac{n_e}{10^{11}\text{ cm}^{-3}}\right)\left(\frac{\ln\Lambda}{20}\right) \quad (6)$$

where n_e is ambient electron density and $\ln\Lambda$ is the Coulomb logarithm (Spitzer 1967). For the impulsive burst, we found no significant energy-dependent variation from the HXR, and we do not believe that the above equation can be used. We however concluded that the MWR electrons belong to a spatially distinct region. If we assume that the MWR variation is governed by Coulomb collisions, and is contributed by electrons in the energy range, 400–900 keV, we then obtain the trap density, $n_e \approx$(4.1–12) $\times 10^9$ cm^{-3}. For the

TABLE 1
DERIVED PHYSICAL PARAMETERS OF THE 2001 APRIL 6 FLARE

Parameters	Impulsive burst	Gradual burst
Individual acceleration time-scale, τ_a [s]	8	30
Interval between acceleration peaks, τ_d [s]	20	60-120
Precipitation rate, ν [10^{-3}s^{-1}]	5–12	2-10
Ratio of injections, $r = Q(> \phi_L)/Q(\leq \phi_L)$	1.5	3.1
Magnetic mirror ratio, B_1/B_2	0.68	0.39
Loss-cone angle, ϕ_L [degree]	39	22
Density in the trap, n_e [10^9 cm^{-3}]	6	0.7

gradual burst, ν decreases with increasing energy, but does not fall as rapid as the Coulomb collision theory predicts. Supposedly another scattering process operates to dominate over the Coulomb collisions at higher energies (Kennel & Petscheck 1966). We thus take the dashed line in the last panel of Figure 5, which meets the Coulomb deflection time scale only at low energies, to estimate the trap density as low as $n_e \approx 6.9 \times 10^8$ cm^{-3}.

The parameter r, that we introduced in Equation (4), represents the ratio of the injected particles inside and outside of the loss cone, namely, the shape of injection pitch angle distribution. However, in case of isotropic pitch angle distribution, r will be just related to the loss cone angle:

$$r = \frac{\pi/2}{\phi_L} - 1 = \frac{\pi/2}{\sin(B_1/B_2)} - 1. \quad (7)$$

For the impulsive burst, we found $r \approx 1.5$, which gives the loss cone angle $\phi_L \approx 39^\circ$ and the magnetic mirror ratio, $B_1/B_2 \approx 0.68$. Such a little variation of magnetic field strength from the loop-top to footpoints is expected for a small loop, which is likely to be the case in view of the separation of the two precipitation points in Figure 2. For the gradual burst, we find $r \approx 3.1$, which corresponds to the loss cone angle $\phi_L \approx 22^\circ$ and the magnetic mirror ratio, $B_1/B_2 \approx 0.39$.

We summarize the results of our analysis in Table 1. It appears that the gradual burst occurred in a region with a lower trap density and a higher magnetic mirror ratio compared with the impulsive burst. This is qualitatively consistent with the conventional idea that gradual bursts should be associated with good trapping condition (e.g., Bai 1986; Kosugi et al. 1988; Melnikov 1990, 1994). However, a more obvious difference between these two types of bursts is found in the acceleration time-scales.

IV. CONCLUSION

In this paper, we have proposed and discussed a kinetic approach for a physical interpretation of MWR and HXR bursts. As an essential part, we have incorporated the presence of finite magnetic field into the trap-and-precipitation system, by which the whole electron population is divided into two components: injection- and trap-related populations. This feature, not available in the classical paradigm, allows us to achieve the goal of separating the acceleration and transport effects.

As a main result of the analysis, we have quantified the acceleration and transport processes in terms of relevant time scales. The acceleration time scale is found as $\tau_a \approx 8$ s for the impulsive bursts and $\tau_a \approx 30$ s for the gradual bursts. The precipitation rate is found as $\nu \approx 1.2 \times 10^{-2}$ s^{-1} for the impulsive flare and $\nu \approx (0.41\text{–}1.1)\times 10^{-2}$ s^{-1} for the gradual bursts depending on energy. Therefore transport effect as gauged by ν found for the HXR-emitting electrons does not show a significant difference between the two bursts. However ν found for the MWR-emitting electrons differs largely from that for the HXR, which can be attributed to the greater sensitivity of MWR to the electrons trapped in the coronal part of the loop than the HXR. Based on imaging we inferred that HXRs should be due to (either direct or indirect) precipitation into thick target, even for the gradual burst. The self-consistency requirement (Eq. [4]) leads us to determine the ratio of the populations of the direct and indirect precipitation, r. If the pitch angle distribution of the injected electrons were isotropic, we can then relate this parameter to the magnetic mirror ratio. In this way we found the magnetic mirror ratio $B_1/B_2 \approx 0.58$ for the impulsive burst, and ≈ 0.3 for the gradual burst. We have also estimated the trap density by comparing the precipitation rate, ν, with the Coulomb deflection time, taking into account some modification by other transport effect. We found $n_e \approx (4.0\text{–}13)\times 10^9$ cm^{-3} for the impulsive burst and $\approx 6.9 \times 10^8$ cm^{-3}.

Although the trap parameters derived in the above show a modest contrast between the two bursts, it remains as a future task as to whether these parameters are sufficient to yield the large difference in the observed flux ratio of HXR to MWR in the impulsive and

gradual solar flares. Specifically, whether or not the lower density and higher magnetic mirror ratio by a factor of 2–5 can entirely explain the microwave excess in the gradual flares needs to be answered. An interesting alternative possibility arises when we interpret r as indicating the degree of anisotropy in the injection pitch angle distribution. If the acceleration occurred in such a way that the parallel momentum distribution prevails in the impulsive burst, and the perpendicular momentum distribution in the gradual burst, we can expect an even more enhanced trapping efficiency in the gradual burst, and this will also help explaining the microwave excess. That the gradual burst shows no signature for the direct precipitation provides another support for such hypothesis of the anisotropic pitch-angle distribution.

In summary, the results of analysis presented in this paper suggest a number of insights into the physical origin of the impulsive and gradual flares. Our result provides quantitative information on the trap condition including magnetic field, density, and precipitation rate, which appears consistent with the traditional idea for the role of trap in creating the gradual nature of solar flares (e.g. Kosugi et al. 1988, Bai 1986). However, the major difference between these two bursts is found not in the trap condition but in the individual acceleration time scale and intermittent period. Further speculation is given here that anisotropy in injection pitch angle may have a profound effect on the dynamic evolution of electrons and the resulting radiative characteristics.

As specific acceleration mechanisms, we can generally think of the DC field acceleration (e.g. Holman 1985, Litvinenko 1996) as suitable for producing the low pitch angle distributions, and thus impulsive flares in the present context, if there indeed forms a field-aligned current during the flares. On the other hand, stochastic accelerations (Hamilton & Petrosian 1992, Miller & Steinacker 1992) are more capable of producing the high pitch-angle distributions, which we inferred for the gradual flares. Applications of these mechanisms to MWR observations were made by Moghaddam-Taaheri & Goertz (1990) and Lee & Gary (1994). To further advance our understanding of electron kinetic processes during solar flare, we therefore suggest to include electron pitch angle distribution in calculation of theoretical MWR spectrum. Such calculation has thus far been not favored, partly due to the computational demand and partly due to the suspicion that anisotropic electron distribution would not last long as an instability develops quickly. However, Fleishman & Melnikov (2003) recently addressed this problem by showing that an anisotropic pitch angle distribution does not always lead to an instability and stably produces a spectral characteristic inherent to its distribution. Future MWR observations and theoretical modeling should make use of such distinctive spectral signatures as additional diagnostic for the electron kinetic process.

ACKNOWLEDGEMENTS

We thank Dr. S. Masuda for help with the Yohkoh data. JL has been supported by NASA grants NAG 5-10891 and NAG-11875. SB thanks support from Ministry of Education in Korea through the US-Korea Cooperative Science Program and the BK21 Program. The OVSA is supported by NSF grant AST-9987366 to NJIT. The X-ray data used in this paper are taken by the *Yohkoh* mission of *ISAS*, Japan.

REFERENCES

Aschwanden, M. J. 1998, Deconvolution of Directly Precipitating and Trap-precipitating Electrons in Solar Flare Hard X-Rays. I. Method and Tests, ApJ, 502, 455

Aschwanden, M. J. 2003, Particle Acceleration and Kinematics in Solar Flares, SPACE SCIENCE REVIEWS, Volume 101, Kluwer Academic Publishers, Dordrecht

Aschwanden, M. J., & Alexander, D. 2001, Flare Plasma Cooling from 30 MK down to 1 MK modeled from Yohkoh, GOES, and TRACE observations during the Bastille Day Event (14 July 2000), Sol. Phys., 204, 93

Aschwanden, M. J., Bynum, R. T., Kosugi, T., Hudson, H., and Schwartz, R.A. 1997, Electron Trapping Times and Trap Densities in Solar Flare Loops Measured with Compton and YOHKOH, ApJ, 487, 936

Aschwanden, M. J., Schwartz, R. A., & Dennis, B. R. 1998, Deconvolution of Directly Precipitating and Trap-precipitating Electrons in Solar Flare Hard X-Rays. II. Compton Gamma Ray Observatory Data Analysis, ApJ, 502, 468

Aschwanden, M. J., Fletcher, L., Sakao, T., Kosugi, T. & Hudson, H. 1999, Deconvolution of Directly Precipitating and Trap-precipitating Electrons in Solar Flare Hard X-Rays. III. Yohkoh Hard X-Ray Telescope Data Analysisi, ApJ, 515, 842

Bai, T. 1982, Transport of energetic electrons in a fully ionized hydrogen plasma, ApJ, 308, 912

Bai, T. 1986, Two classes of gamma-ray/proton flares - Impulsive and gradual, ApJ, 308, 912

Bai, T. & Ramaty, R. 1979, Hard X-ray time profiles and acceleration processes in large solar flares, ApJ, 227, 1072

Bai, T. & Sturrock, P. A., 1989, Classification of solar flares, ARA&A, 27, 421

Bruggmann, G., Vilmer, N., Klein, K.-L., & Kane, S. R. 1994, Electron trapping in evolving coronal structures during a large gradual hard X-ray/radio burs, Sol. Phys., 149, 171

Cornell, M. E., Hurford, G. J., Kiplinger, A. L., & Dennis, B. R. 1984, The relative timing of microwaves and hard X-rays in solar flares, ApJ, 279, 875

Crannell, C. J., Frost, K. J., Saba, J. L., Maetzler, C. & Ohki, K. 1978, Impulsive solar X-ray bursts, ApJ, 223, 620

Ding, M. D., Qiu, J., & Wang, H. 2002, Non-LTE Calculation of the Ni I 676.8 Nanometer Line in a Flaring Atmosphere, ApJ, 576, L83

Fleishman, G. D. & Melnikov, V. F. 2003, Gyrosynchrotron Emission from Anisotropic Electron Distribution, ApJ, 587, 823

Gary, D. E. & Hurford, G. J. 1999, OVRO Solar Array Upgrades in Preparation for MAX 2000 in Proceedings of the Nobeyama Symposium, held in Kiyosato, Japan, Oct. 27-30, 1998, (Eds.) T. S. Bastian, N. Gopalswamy and K. Shibasaki, NRO Report No. 479., p.429-432

Hamilton, R. J. & Petrosian, V. 1992, Stochastic acceleration of electrons. I - Effects of collisions in solar flares, ApJ, 398, 350

Hanaoka, Y. 1996, Flares and Plasma Flow Caused by Interacting Coronal Loops, Sol. Phys., 165, 275

Hanaoka, Y. 1997, Double-Loop Configuration of Solar Flares, Sol. Phys., 173, 319

Holman, G. D. 1985, Acceleration of runaway electrons and Joule heating in solar flares, ApJ, 293, 584

Holman, G. D., Kundu, M. R., & Papadopoulos, P. 1982, Electron pitch angle scattering and the impulsive phase microwave and hard X-ray emission from solar flares, ApJ, 257, 354

Kai., K. 1986, Can observed hard X-ray and microwave flux from solar flares be explained by a single electron population?, Sol. Phys., 104, 235

Kai, K. Kosugi, T., & Nitta, N. 1985, Flux relations between hard X-rays and microwaves for both impulsive and extended solar flares, PASP, 37, 155

Kennel, C. F. & Petscheck, H. E. 1966, Limit on stably trapped particle fluxes, J. Geophys. Res., 71, 1

Klein, K.-L., Trottet, G., & Magun, A. 1986, Microwave diagnostics of energetic electrons in flare, Sol. Phys., 104, 243

Kosugi, T., Dennis, B. R., & Kai, K. 1988, Energetic electrons in impulsive and extended solar flares as deduced from flux correlations between hard X-rays and microwave, ApJ, 324, 1118

Kosugi, T., Masuda, S., Makishima, K., Inda, M., Murakami, T., Dotani, T., Ogawara, Y., Sakao, T., Kai, K., & Nakajima, H. 1991, The hard X-ray telescope (HXT) for the Solar-A mission, Sol. Phys., 136, 17

Kundu, M. R., White, S. M., Shibasaki, K., Sakurai, T., & Grechnev, V. V. 2001a, Spatial Structure of Simple Spiky Bursts at Microwave/Millimeter Wavelengths, ApJ, 547, 1090

Kundu, M. R., Grechnev, V. V., Garaimov, V. I., & White, S. M. 2001b, Double Loop Configuration of a Flaring Region from Microwave, Extreme-Ultraviolet, and X-Ray Imaging Data, ApJ, 563, 389

Kundu, M. R., Nitta, N., White, S. M., Shibasaki, K., Enome, S., Sakao, T., Kosugi, T., & Sakurai, T. 1995, Microwave and Hard X-Ray Observations of Footpoint Emission from Solar Flares, ApJ, 454, 522

Lee, J. & Gary, D. E. 1994, Spectral evolution of microwaves and hard X-rays in the 1989 March 18 flare and its interpretation, Sol. Phys., 153, 347

Lee, J. & Gary, D. E. 2000, Solar Microwave Bursts and Injection Pitch-Angle Distribution of Flare Electrons, ApJ, 543, 457

Lee, J., Gary, D. E., & Zirin, H. 1994, Flat microwave spectra seen at X-class flare, Sol. Phys., 152, 409

Lee, J., Gary, D. E., & Shibasaki, K. 2000, Magnetic Trapping and Electron Injection in Two Contrasting Solar Microwave Bursts, ApJ, 531, 1109

Lee, J., Gary, D. E., Qiu, J., & Gallagher, P. T. 2002, Electron Transport during the 1999 August 20 Flare Inferred from Microwave and Hard X-Ray Observations, ApJ, 572, 609

Lee, J., Gallagher, P. T., Gary, D. E., Nita, G. M., Choe, G. S., Bong, S.-C., & Yun, H. S. 2003, H-alpha;, Extreme-Ultraviolet, and Microwave Observations of the 2000 March 22 Solar Flare and Spontaneous Magnetic Reconnection, ApJ, 585, 524

Litvinenko, Y. E. 1996, Particle Acceleration in Reconnecting Current Sheets with a Nonzero Magnetic Field, ApJ, 462, 997

Lu, E. T. and Petrosian, V. 1988, Rapid temporal evolution of radiation from nonthermal electrons in solar flares, ApJ, 327, 405

MacKinnon, A. L. 1991, Collisional scattering of fast electrons in a coronal magnetic bottle, A&A, 242, 256

Marsh, K. A. & Hurford, G. J., 1982, High spatial resolution solar microwave observations, ARA&A, 20, 497

Melnikov, V. F. 1990, Relationships between Microwave, Hard X ray, and Corpuscular Emissions of Solar Flares, Ph.D. Thesis, Radiophysical Research Institute, Nizhniy Novgorod, Russia

Melnikov, V. F. 1994, Particle Acceleration and Capturing in Impulsive and Gradual Bursts, Radiophys. Quant. Electron. 37, 557

Melnikov, V. F. & Magun, A. 1998, Spectral Flattening During Solar Radio Bursts At Cm-mm Wavelengths and the Dynamics of Energetic Electrons in a Flare Loop, Sol. Phys., 178, 153

Melnikov, V. F., Shibasaki, K., & Reznikova, V. E. 2002, Loop-Top Nonthermal Microwave Source in Extended Solar Flaring Loops, ApJ, 580, L85

Melrose, D. B. 1980, Plasma Astrophysics, (New York: Gordon and Breach)

Melrose, D. B. & Brown, J. C. 1976, Precipitation in trap models for solar hard X-ray bursts, MNRAS, 176, 15

Miller, J. A. & Steinacker, J. 1992, Stochastic gyroresonant electron acceleration on a low-beta plasma. II - Implications of thermal effects in a solar flare plasma, ApJ, 399, 284

Miller, J. A., Cargill, P. J., Emslie, A. G., Holman, G. D., Dennis, B. R., LaRosa, T. N., Winglee, R. M., Benka, S. G., & Tsuneta, S. 1997, Critical Issues For Understanding Particle Acceleration in Impulsive Solar Flares, J. Geophys. Res., 102, 14631

Moghaddam-Taaheri, E. & Goertz, C. K. 1990, Acceleration of runaway electrons in solar flares, ApJ, 352, 361

Nishio, M., Yaji, K., Kosugi, T., Nakajima, H., & Sakurai, T. 1997, Magnetic Field Configuration in Impulsive Solar Flares Inferred from Coaligned Microwave/X-Ray Images, ApJ, 489, 976

Petrosian, V. 1982, Structure of the impulsive phase of solar flares from microwave observations, ApJ, 255, L85

Petrosian, V. 1990, Acceleration, transport of and radiation by electrons in impulsive phase of flares, in Basic plasma processes on the sun (A92-30901 12-92). Dordrecht, Netherlands, Kluwer Academic Publishers, p. 391

Ramaty, R. 1969, Gyrosynchrotron Emission and Absorption in a Magnetoactive Plasma, ApJ, 158, 753

Sakao, T. 1994, Characteristics of solar flare hard X-ray sources as revealed with the Hard X-ray Telescope aboard the Yohkoh satellite, Ph.D. thesis, University of Tokyo

Scherrer, P. H., et al. 1995, The Solar Oscillations Investigation - Michelson Doppler Imager, Sol. Phys., 162, 129

Silva, A. V. R., Wang, H., & Gary, D. E. 2000, Correlation of Microwave and Hard X-Ray Spectral Parameters, ApJ, 545, 1116

Spitzer, L. 1967, The Physics of Fully Ionized Gases (2d ed., New York: Interscience)

Takakura, T. & Kai. K. 1966, Energy Distribution of Electrons Producing Microwave Impulsive Bursts and X-Ray Bursts from the Sun, PASJ 18, 57

Vilmer, N., Kane, S. R., & Trottet, G. 1982, mpulsive and gradual hard X-ray sources in a solar flare, A&A, 108, 306

Yoshimori, M., Okudaira, K., Hirasima, Y., Igarashi, T., Akasaka, M., Takai, Y., Morimoto, K., Watanabe, T., Ohki, K., & Nishimura, J. 1991, The wide band spectrometer on the Solar-A, Sol. Phys., 136, 69

Zirin, H. & Tanaka, K. 1981, Magnetic transients in flares, ApJ, 250, 791